



**HAL**  
open science

## Tidal instability in stellar and planetary binary systems

M. Le Bars, Laurent Lacaze, S. Le Dizès, P. Le Gal, M. Rieutord

► **To cite this version:**

M. Le Bars, Laurent Lacaze, S. Le Dizès, P. Le Gal, M. Rieutord. Tidal instability in stellar and planetary binary systems. *Physics of the Earth and Planetary Interiors*, 2010, 178 (1-2), pp.48-55. 10.1016/j.pepi.2009.07.005 . hal-00601517

**HAL Id: hal-00601517**

**<https://hal.science/hal-00601517>**

Submitted on 18 Jun 2011

**HAL** is a multi-disciplinary open access archive for the deposit and dissemination of scientific research documents, whether they are published or not. The documents may come from teaching and research institutions in France or abroad, or from public or private research centers.

L'archive ouverte pluridisciplinaire **HAL**, est destinée au dépôt et à la diffusion de documents scientifiques de niveau recherche, publiés ou non, émanant des établissements d'enseignement et de recherche français ou étrangers, des laboratoires publics ou privés.

## Accepted Manuscript

Title: Tidal instability in stellar and planetary binary systems

Authors: M. Le Bars, L. Lacaze, S. Le Dizès, P. Le Gal, M. Rieutord

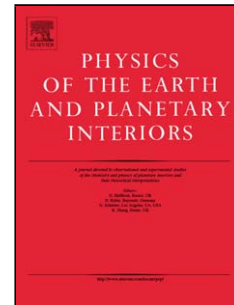
PII: S0031-9201(09)00148-4  
DOI: doi:10.1016/j.pepi.2009.07.005  
Reference: PEPI 5180

To appear in: *Physics of the Earth and Planetary Interiors*

Received date: 18-12-2008  
Revised date: 20-5-2009  
Accepted date: 1-7-2009

Please cite this article as: Le Bars, M., Lacaze, L., Le Dizès, S., Le Gal, P., Rieutord, M., Tidal instability in stellar and planetary binary systems, *Physics of the Earth and Planetary Interiors* (2008), doi:10.1016/j.pepi.2009.07.005

This is a PDF file of an unedited manuscript that has been accepted for publication. As a service to our customers we are providing this early version of the manuscript. The manuscript will undergo copyediting, typesetting, and review of the resulting proof before it is published in its final form. Please note that during the production process errors may be discovered which could affect the content, and all legal disclaimers that apply to the journal pertain.



# Tidal instability in stellar and planetary binary systems

M. Le Bars<sup>\*,a</sup>, L. Lacaze<sup>b</sup>, S. Le Dizès<sup>a</sup>, P. Le Gal<sup>a</sup>, M. Rieutord<sup>c</sup>

<sup>a</sup>*Institut de Recherche sur les Phénomènes Hors Equilibre, UMR 6594, CNRS et Aix-Marseille Université, 49 rue F. Joliot-Curie, BP146, 13384 Marseille Cédex 13, France.*

<sup>b</sup>*Institut de Mécanique des Fluides de Toulouse, CNRS et Université de Toulouse, 1 Allée du Professeur Camille Soula, 31400 Toulouse, France.*

<sup>c</sup>*Laboratoire d'Astrophysique de Toulouse-Tarbes, CNRS et Université de Toulouse, 14 avenue E. Belin, 31400 Toulouse, France*

---

## Abstract

In this paper, we combine theoretical and experimental approaches to study the tidal instability in planetary liquid cores and stars. We demonstrate that numerous complex modes can be excited depending on the relative values of the orbital angular velocity  $\Omega_{orbit}$  and of the spinning angular velocity  $\Omega_{spin}$ , except in a stable range characterized by  $\Omega_{spin}/\Omega_{orbit} \in [-1; 1/3]$ . Even if the tidal deformation is small, its subsequent instability - coming from a resonance process - may induce motions with large amplitude, which play a fundamental role at the planetary scale. This general conclusion is illustrated in the case of Jupiter's moon Io by a coupled model of synchronization, demonstrating the importance of energy dissipation by elliptical instability.

*Key words:* tides, tidal/elliptical instability, synchronization, binary systems

---

<sup>\*</sup>corresponding author

*Email address:* lebars@irphe.univ-mrs.fr (M. Le Bars)

## 1 **1. Introduction**

2 The fundamental role of tides in geo- and astrophysics has been the sub-  
3 ject of multiple studies for more than four centuries. Beyond the well-known  
4 quasi-periodic flow of ocean water on our shores, tides are also responsible for  
5 phenomena as varied as the intense volcanism on Io or the synchronization  
6 of the Moon on Earth. In stars and liquid planetary cores, tides may also  
7 excite an hydrodynamic "elliptical" instability, whose consequences are not  
8 yet fully understood. The purpose of the present work is twofold: we shall  
9 first systematically characterize the excited modes of the elliptical (or tidal)  
10 instability in a rotating spheroid depending on its orbital and spinning veloc-  
11 ities, and then demonstrate the importance of this instability in stellar and  
12 planetary binary systems using a simplified but illustrative model of tidal  
13 synchronization.

14 The elliptical instability, whose existence is related to a parametric reso-  
15 nance of inertial waves, is well-known in aeronautics, and more generally in  
16 the field of vortex dynamics: it actually affects any rotating fluid, as soon as  
17 its streamlines are elliptically deformed. Since its discovery in the mid-1970s,  
18 the elliptical instability has received considerable attention, theoretically, ex-  
19 perimentally and numerically (see for instance the review by Kerswell, 2002).  
20 Its presence in planetary and stellar systems, elliptically deformed by gravi-  
21 tational tides, has been suggested for several years. It could for instance be  
22 responsible for the surprising existence of a magnetic field in Io (Kerswell and  
23 Malkus, 1998; Lacaze et al., 2006; Herreman et al., 2009) and for fluctuations  
24 in the Earth's magnetic field on a typical timescale of 10,000 years (Aldridge  
25 et al., 1997). It may also have a significant influence on the evolution of

26 binary stars (e.g. Rieutord, 2003).

27 In all these studies, it is assumed that the tidal deformation is fixed and  
28 that the excited resonance is the so-called spin-over mode, which corresponds  
29 to a solid body rotation around an axis inclined compare to the spin axis of  
30 the system. This is indeed the only perfect resonance in spherical geometry  
31 in the absence of rotation of the elliptical deformation (Lacaze et al., 2004).  
32 But in all natural configurations such as binary stars, moon-planet systems  
33 or planet-star systems, orbital motions are also present, which means that  
34 the gravitational interaction responsible for the tidal deformation is rotating  
35 with an angular velocity and/or a direction different from the spin of the  
36 considered body. This significantly changes the conditions for resonance  
37 and the mode selection process, as recently demonstrated in the cylindrical  
38 geometry (Le Bars et al., 2007).

39 The paper is organized as follow. In section 2, in complement to the  
40 trends presented in Le Bars et al. (2007), we systematically characterize the  
41 excited modes of the elliptical instability in a rotating spheroid depending on  
42 its orbital and spinning velocities, using both theoretical and experimental  
43 approaches. We then describe in section 3 a fully coupled simplified model of  
44 synchronization of stellar and planetary binary systems, demonstrating the  
45 importance of energy dissipation by elliptical instability. In the last section,  
46 the main results of the paper are summarized and general conclusions for  
47 geo- and astrophysical systems are briefly discussed.

48 **2. Excited modes of the elliptical instability in an orbiting spinning**  
 49 **spheroid**

50 Our study is based on the laboratory experiment shown in figure 1a.  
 51 The set-up consists in a deformable and transparent hollow sphere of radius  
 52  $R = 2.175\text{cm}$ , set in rotation about its axis ( $Oz$ ) with an angular velocity  
 53  $\Omega_F$  up to  $\pm 300\text{rpm}$ , simultaneously deformed elliptically by two fixed rollers  
 54 parallel to ( $Oz$ ). The container is filled with water seeded with anisotropic  
 55 particles (Kalliroscope). For visualization, a light sheet is formed in a plane  
 56 coinciding with the rotation axis, allowing the measurement of wavelengths  
 57 and frequencies of excited modes. The whole set-up is placed on a 0.5m-  
 58 diameter rotating table allowing rotation with an angular velocity  $\Omega_{orbit}$  up  
 59 to 60rpm. Such a system is fully defined by three dimensionless numbers:  
 60  $\varepsilon$ , the eccentricity of the tidal deformation,  $\Omega = \Omega_{orbit}/\Omega_F$ , the ratio be-  
 61 tween the orbital and the fluid angular velocities, and  $E = \nu/\Omega_F R^2$ , an  
 62 Ekman number, where  $\nu$  is the kinematic viscosity of the fluid. In geo- and  
 63 astrophysical terms, this toy model mimics a tidally deformed fluid body  
 64 spinning at  $\Omega_{spin} = \Omega_F + \Omega_{orbit}$  with a tidal deformation rotating at the or-  
 65 bital velocity  $\Omega_{orbit}$  (see figure 1b). Note that in natural configurations, the  
 66 gravitational interactions responsible for the boundary deformation of the  
 67 considered planet or star also act over the whole depth of the system. This  
 68 feature cannot be taken into account in our toy model. However, it touches  
 69 another side of the problem, namely the role of compressibility and stratifica-  
 70 tion which we leave for subsequent studies. We focus here on incompressible  
 71 effects only, considering a fluid of uniform density.

72 *2.1. Linear global analysis*

73 As previously mentioned, the elliptical instability is generated by the  
 74 parametric resonance of two normal modes of the undistorted circular flow  
 75 with the underlying strain field (e.g. Waleffe, 1990; Kerswell, 2002). We have  
 76 thus performed a so-called "global" analysis of the instability, which consists  
 77 in (i) determining the normal modes of the sphere, (ii) calculating explicitly  
 78 the conditions for resonance, which immediately provides information on the  
 79 structure of the selected instability and (iii) determining the growth rate of  
 80 this instability. In the following, we work in the frame rotating with the ro-  
 81 tating table (i.e. in the frame where the elliptical deformation is stationary),  
 82 and variables are nondimensionalized using the characteristic lengthscale  $R$   
 83 and the characteristic timescale  $1/\Omega_F$  (i.e. the relevant timescale for the  
 84 elliptical instability, corresponding to the differential rotation of the fluid  
 85 compared to the elliptical deformation).

86 As explained in Le Bars et al. (2007), inviscid normal modes in a rotating  
 87 container submitted to a global rotation  $\Omega$  are related to inviscid normal  
 88 modes without global rotation through the relation

$$\{\mathbf{u}, p\}(\omega, \Omega, m, l) = \left\{ \frac{\mathbf{u}}{1 + \Omega}, p \right\}(\tilde{\omega}, 0, m, l) \quad (1)$$

89 where  $\mathbf{u}$  and  $p$  stand for the velocity and the pressure respectively. Here,  
 90  $\omega$  is the mode frequency in the frame rotating with the elliptical deforma-  
 91 tion,  $\tilde{\omega} = (\omega + m\Omega)/(1 + \Omega)$ , and  $m$  and  $l$  are azimuthal and "meridional"  
 92 wavenumbers respectively (see Lacaze et al., 2004, for details). Due to this  
 93 property, the dispersion relation solutions in the sphere with global rotation  
 94 are the same as the ones given by Lacaze et al. (2004) without global rotation

95 when  $\omega$  is replaced by  $\tilde{\omega}$ . The linear analysis of the elliptical instability in  
 96 the rotating frame can thus be expressed from the results obtained without  
 97 global rotation. The condition for resonance between two waves is simply  
 98 given by  $(m_2, \omega_2) = (m_1 + 2, \omega_1)$ , and the corresponding excited resonance is  
 99 labeled by  $(m_1, m_2)$ . Note that as frequencies of normal modes are confined  
 100 to the interval  $m - 2 < \tilde{\omega} < m + 2$ , resonances are only possible for  $\Omega$  outside  
 101 the range  $[-3/2; -1/2]$ . There, the growth rate  $\sigma_1 = \sigma/\varepsilon$  is solution of the  
 102 equation (see again Lacaze et al., 2004, for details)

$$\begin{aligned} & \left( \sigma_1 \tilde{\mathcal{J}}_{1|1} - \sqrt{E} \nu_s^1 (1 + \Omega)^2 / \varepsilon - \tilde{\mathcal{C}}_{1|1} \right) \left( \sigma_1 \tilde{\mathcal{J}}_{2|2} - \sqrt{E} \nu_s^2 (1 + \Omega)^2 / \varepsilon - \tilde{\mathcal{C}}_{2|2} \right) \\ & = \left( \tilde{\mathcal{N}}_{1|2} - (1 + \Omega) \tilde{I}_1 \right) \left( \tilde{\mathcal{N}}_{2|1} - (1 + \Omega) \tilde{I}_2 \right), \end{aligned} \quad (2)$$

103 where  $\tilde{\mathcal{J}}_{i|i}$  corresponds to the norm of mode  $i$ ,  $\tilde{\mathcal{N}}_{i|j}$  to the coupling coefficient  
 104 between modes  $i$  and  $j$ ,  $\nu_s^i$  to the viscous damping induced by the no-slip  
 105 boundary condition on each mode derived from the work of Kudlick (1966)<sup>1</sup>,  
 106 and  $\tilde{\mathcal{C}}_{i|i}$  to the possible detuning of the instability when  $\Omega$  is slightly off the  
 107 perfect resonance condition. The exact expressions of all these coefficients  
 108 are given in appendix A.

109 Numerical resolution of equation (2) determines the growth rate of any  
 110 given resonance depending on the dimensionless parameters  $(\varepsilon, \Omega, E)$ . Our  
 111 computations demonstrate that only principal resonances characterized by  
 112 the same meridional wavenumber (i.e.  $l_1 = l_2$ ) lead to a significant posi-  
 113 tive growth rate, as already noted for non-rotating cases by Kerswell (1993)

---

<sup>1</sup>Note that only boundary layer effects are considered here, and that damping due to inner shear layers are neglected. This assumption has been fully justified by numerical computation for the spin-over mode (Hollerbach and Kerswell, 1995), and is supposed to remain valid here.



114 and Lacaze et al. (2004). An example of the resolution of equation (2) as a  
 115 function of  $\Omega$  is shown in figure 2(a) for the parameter range relevant to our  
 116 experimental configuration. Each mode can be excited inside a resonance  
 117 band in  $\Omega$  where the growth rate is positive. When several resonances are  
 118 possible at a given value of  $\Omega$ , one expect the most unstable mode (i.e. the  
 119 one with the largest growth rate) to be the first one excited. We also show  
 120 in figures 2(b) and 2(c) the effects of eccentricity and Ekman number: de-  
 121 creasing  $\varepsilon$  implies narrower resonance bands, whereas decreasing the Ekman  
 122 number allows the excitation of more resonances. In the limit of small Ekman  
 123 numbers relevant to planetary and stellar systems, we find that there always  
 124 exists an excitable resonance, except in the stable range  $\Omega \in [-3/2; -1/2]$ ,  
 125 corresponding in astrophysical terms to  $\Omega_{spin}/\Omega_{orbit} \in [-1; 1/3]$ . Besides, as  
 126 shown in figure 2(c), its growth rate is correctly approximated by

$$\sigma_1 = \frac{(3 + 2\Omega)^2}{16(1 + \Omega)^2} - c \frac{\sqrt{E}}{\varepsilon}, \quad (3)$$

127 where the first term on the right-hand side comes from the inviscid local  
 128 analysis (Le Dizès, 2000) and where  $c$  is a constant of order 1, which can be  
 129 explicitly computed for each resonance using equation (2).

## 130 2.2. Experimental results

131 A series of experiments was performed with a fixed eccentricity  $\varepsilon = 0.16$   
 132 and various Ekman numbers in the range  $[10^{-5}; 10^{-4}]$ , systematically chang-  
 133 ing  $\Omega_{orbit}$  and  $\Omega_F$  to excite various resonances. Starting from rest, we first  
 134 set the table's rotation to its assigned value  $\Omega_{orbit}$ . Once solid body rotation  
 135 is reached, the second motor controlling the fluid rotation is turned on. We

136 then observe the potential development of an instability using a video cam-  
 137 era embedded on the table. As illustrated in figure 2(a), good agreement  
 138 with the global analysis is found regarding the selected resonance: outside  
 139 the stable range  $\Omega \in [-3/2; -1/2]$ , stationary  $(-1, 1)$  mode with a sinusoidal  
 140 rotation axis and various wavelengths as well as other more exotic modes rec-  
 141 ognized by their complex radial structure and/or by their periodic behavior  
 142 (see figures 3 and 4) can be selected by changing the dimensionless ratio  $\Omega$   
 143 only, providing the Ekman number is small enough. For each selected value  
 144 of  $\Omega$ , the first observed mode of instability corresponds to the most unstable  
 145 mode by the theory (i.e. the one with the largest growth rate). In the vicin-  
 146 ity of the threshold, the excited resonance induces a flow whose saturation  
 147 amplitude rapidly grows with  $\varepsilon$  and  $\Omega_F R$ , until reaching a value comparable  
 148 to the imposed rotation velocity  $\Omega_F R$  (see for instance figure 5). At slightly  
 149 smaller Ekman numbers or slightly larger  $\varepsilon$ , we then observe disordered pat-  
 150 terns superimposed on the selected main flow (figure 5c,d). These patterns  
 151 may induce the collapse of the selected mode on a very rapid timescale com-  
 152 parable to the rotation rate, and an intermittent behavior takes place. When  
 153 several theoretical resonances are close to each other, we observed complex  
 154 patterns originating from the superimposition or the succession in time of  
 155 the different modes.

156 Note again that in the absence of global rotation, the only perfect res-  
 157 onance and the first destabilized mode in the vicinity of threshold is the  
 158 spin-over mode. This is the first time that oscillatory modes such as the  
 159  $(0, 2)$  one shown in figures 3 and 4a and the  $(1, 3)$  one shown in figure 4b are  
 160 experimentally observed in a sphere.

161 *2.3. Estimates of power dissipation*

162 Energy dissipated by tides in a planet is traditionally related to the dis-  
163 sipation of the induced shear flow by viscosity in its fluid part(s) and by  
164 anelasticity in its solid part(s): it is thus typically proportional to the square  
165 of the (small) tidal deformation  $\varepsilon$ . With the exception of Earth, where the  
166 prevalent source of dissipation is due to viscous friction of water tides on  
167 ocean floor (estimated power  $2 \times 10^{12}W$ ), the fluid component of tidal dis-  
168 sipation usually remains negligible. However, we observe in our experiments  
169 that even if the tidal deformation is very small, its subsequent instability  
170 induces a flow over the whole system with a typical velocity comparable to  
171 the imposed rotation velocity  $\Omega_F R$ , as soon as  $\varepsilon/\sqrt{E}$  is about 10 (see for  
172 instance figure 5 and the analytical model by Lacaze et al. (2004)). This is  
173 especially important when trying to estimate the energy dissipated by the  
174 elliptical instability.

175 Schematically, the intermittent behavior observed at small Ekman num-  
176 bers in our experiment can be characterized by three stages. First, starting  
177 from the base flow (which can be either a laminar solid body rotation or a  
178 more turbulent state induced for instance by convection or differential ro-  
179 tation), the instability grows continuously on a typical time given by the  
180 growth rate, until it saturates to a typical velocity. Then, the selected mode  
181 breaks down into small scales in a very short timescale, comparable to some  
182 fluid's rotations and significantly smaller than the typical growth time of the  
183 instability (see also Lacaze et al., 2004). A new cycle then begins. Note that  
184 the energy dissipation related to this collapse has already been evaluated by  
185 several authors (Malkus, 1968; Vanyo, 1991; Kerswell, 1996; Kerswell and

186 Malkus, 1998) and leads to the estimate  $P_{dissip} \sim \rho R^5 \Omega_F^3$  (this would corre-  
 187 spond to an unrealistically huge amount of dissipation during the collapse  
 188 breakdown, e.g.  $P_{dissip} \sim 2 \times 10^{24} W$  in the Earth, but see the relevant dis-  
 189 cussion in Kerswell and Malkus (1998)). In the context of this paper, we  
 190 focus on the continuous viscous dissipation during growth and saturation of  
 191 the instability.

192 The energy necessary to excite and maintain the selected mode is supplied  
 193 by the tidal deformation and by the relative angular velocity of the spherical  
 194 container (i.e. the rigid mantle in the case of a planet) compared to tides.  
 195 Following the model of Vanyo and Likins (1972) developed in the closely  
 196 related case of precession, one may consider that this energy is transmitted  
 197 to the fluid (i.e. the liquid core in the case of a planet) through a thin  
 198 viscous boundary layer at the solid-liquid interface. In the absence of orbital  
 199 velocity, the spin-over mode takes place, similarly to the case of precession,  
 200 and we may consider the "rigid sphere approximation" introduced in Vanyo  
 201 and Likins (1972): the interior portion of the fluid is assumed to behave as  
 202 a perfectly rigid sphere rotating at  $\Omega_{spin} + \Omega_{SO}$ , where  $\Omega_{SO}$  is the spin-over  
 203 mode. The moment of the container acting on the fluid can then be expressed  
 204 as

$$\mathbf{C}^{m/c} = -2M\nu \frac{R}{h} \Omega_{SO}, \quad (4)$$

205 where  $M$  is the mass of the fluid and  $h$  the size of the viscous boundary layer,  
 206 taken as  $h = \sqrt{\nu/\Omega_{SO}}$ . The power dissipated by the whole system (i.e. the  
 207 container rotating at  $\Omega_{spin}$  plus the fluid rotating at  $\Omega_{spin} + \Omega_{SO}$ ) is then  
 208 simply given by

$$P_{ell} = \Omega_{SO} \cdot \mathbf{C}^{m/c} = -2M\nu \frac{R}{h} \Omega_{SO}^2, \quad (5)$$

209 Replacing  $\Omega_{SO}$  by  $\Omega_{spin}\omega_{SO}$ , where  $\omega_{SO}$  is the dimensionless spin-over mode  
 210 amplitude which typically ranges between 0 (below threshold of the tidal  
 211 instability) and 1 (far from threshold of the tidal instability), the dissipated  
 212 power is written

$$P_{ell} = -2MR\sqrt{\nu}|\Omega_{spin}|^{5/2}|\omega_{SO}|^{5/2}. \quad (6)$$

213 The non-linear evolution of  $\omega_{SO}$  as a function of time and its dependence  
 214 on  $\varepsilon$  and  $E$  have been modeled theoretically by Lacaze et al. (2004) for the  
 215 laminar mode, in close agreement with experimental results. We are thus in  
 216 position to evaluate the energy dissipation  $P_{ell}$  for the spin-over mode. In  
 217 the more general case where orbital velocity is present, the energy necessary  
 218 for the instability comes from the difference between the spin velocity and  
 219 the rotation velocity of the tides (i.e. the orbital velocity) and one may  
 220 reasonably expect the dissipated power to be

$$P_{ell} = -2M\sqrt{\nu}|\Omega_{spin} - \Omega_{orbit}|^{5/2}|\omega_{ell}|^{5/2}. \quad (7)$$

221 Here,  $\omega_{ell}$  is the dimensionless amplitude of the selected resonance, which  
 222 should be comparable to the amplitude of the spin-over mode for the same  
 223 values of eccentricity and Ekman number. Note that at large value of  $\varepsilon$  or  
 224 small value of  $E$ , this calculation will represent a lower bound, since it does  
 225 not take into account the additional turbulent dissipation coming from the  
 226 chaotic motions superimposed on the large scale mode (see figure 5).

227 Evaluation of  $P_{ell}$  for the Earth is difficult because its core is just at the  
 228 vicinity of the threshold for instability, where  $\omega_{ell}$  rapidly changes from 0 to  
 229 1 (Lacaze et al., 2006). Following Aldridge et al. (1997), if we suppose that  
 230 the growth rate of the instability is correctly approximated by the classical

231 formula  $\sigma = 0.5\epsilon - 2.62\sqrt{E}$  and that the typical growth rate of the instability  
 232 in the Earth ranges between  $10^3$  and  $10^6$  years, the dissipation due to the  
 233 (laminar) tidal instability ranges between  $P_{ell} \sim 10^9 W$  and  $P_{ell} \sim 2 \times 10^5 W$   
 234 respectively. It thus remains relatively small compared to the viscous dissipa-  
 235 tion by water tides on ocean floor (typically  $2 \times 10^{12} W$ ), which is supposed to  
 236 be the dominant effect in the case of the Earth. Let us now look at Jupiter's  
 237 moon Io. As explained for instance in Kerswell and Malkus (1998), Io is  
 238 almost synchronized in its revolution around Jupiter, but orbital resonances  
 239 with Europa and Ganymede force it to follow a slightly elliptical orbit of  
 240 eccentricity  $\beta = 0.004$ . As a result, the tidal bulge raised by Jupiter, of  
 241 magnitude  $\epsilon \sim 6 \times 10^{-3}$ , oscillates back and forth across Io's body with a  
 242 typical angular velocity  $\Omega_{orbit} = \Omega_{spin}(1 - 2\beta \cos(\Omega_{spin}t))$ . With the charac-  
 243 teristic values for Io tides given by Kerswell and Malkus (1998), one then  
 244 finds that the elliptical instability almost saturates at its maximum value  
 245 (i.e.  $\omega_{ell} = 0.99$ ) and  $P_{ell} \sim 4 \times 10^9 W$  at saturation, i.e. a large dissipation  
 246 for fluid motion, but negligible compared to the estimated tidal dissipation in  
 247 Io's mantle (i.e.  $O(10^{14})W$ ). However this value corresponds to the present  
 248 state of Io (i.e. almost synchronized) and does not preclude that tidal dissi-  
 249 pation may have had a first order influence in the past, especially during its  
 250 evolution towards synchronization.

### 251 **3. A fully coupled model of synchronization of stellar and planetary** 252 **binary systems**

253 Our theoretical study, confirmed by laboratory experiments, highlights  
 254 several points directly relevant to synchronizing stellar and planetary binary

255 systems. Provided that  $\sqrt{E}/\epsilon \ll 1$  (which is usually the case for moons  
 256 and close binary stars, and which may be the case for some planetary cores),  
 257 we conclude from the previous section that (i) a mode of the elliptical insta-  
 258 bility will always be excited, except when  $\Omega_{spin}/\Omega_{orbit} \in [-1; 1/3]$ , that (ii)  
 259 its growth rate is correctly approximated by equation (3) with a constant  
 260  $1 < c < 10$ , that (iii) the induced fluid motion may take various and complex  
 261 forms, and that (iv) the tidal instability may generate first order motions.  
 262 As opposed to our experiments where spinning and orbital angular velocities  
 263 are imposed by two motors, the energy dissipation related to these motions  
 264 in natural configuration implies an evolution of the binary system towards  
 265 synchronization. To further illustrate and quantify this effect, we now exam-  
 266 ine a fully coupled model of tidal synchronization based on our theoretical  
 267 and experimental results. Note again that in the limit  $\sqrt{E}/\epsilon \ll 1$ , reso-  
 268 nance bands are dense in the  $\Omega_{spin}/\Omega_{orbit}$  space, except in the stable range  
 269  $\Omega_{spin}/\Omega_{orbit} \in [-1; 1/3]$ . We thus suppose that during the evolution, the in-  
 270 stability jumps from one resonance band to the following one while always  
 271 remaining at saturation. In particular, we do not consider any cyclic behav-  
 272 ior with growing and breakdown phases of the instability, as observed in our  
 273 experiments with unaltered forcing.

274 We consider two spinning bodies of radius  $R_i$  and mass  $M_i$  orbiting on  
 275 a circular trajectory of radius  $a$ . We note  $I_i$  and  $\Omega_{spin,i}$  the moment of  
 276 inertia and the angular velocity of the mantle of body  $i$ , and  $I_{core,i}$  and  
 277  $\Omega_{core,i}$  the moment of inertia and the angular velocity of the core of body  $i$ .  
 278 The tidal deformation of body 1 by body 2 is given in the limit of hydrostatic  
 279 equilibrium by  $\epsilon = \frac{3}{2} \frac{M_2}{M_1} \left(\frac{R_1}{a}\right)^3$ . The evolution of this system is described by

280 two coupled equations, corresponding to the conservation of total angular  
281 momentum

$$L = \frac{M_1 M_2}{M_1 + M_2} a^2 \Omega_{orbit} + I_1 \Omega_{spin,1} + I_{core,1} \Omega_{core,1} + I_2 \Omega_{spin,2} + I_{core,2} \Omega_{core,2}, \quad (8)$$

282 and to the decrease of mechanical energy

$$E = -\frac{GM_1 M_2}{2a} + \frac{1}{2} I_1 \Omega_{spin,1}^2 + \frac{1}{2} I_{core,1} \Omega_{core,1}^2 + \frac{1}{2} I_2 \Omega_{spin,2}^2 + \frac{1}{2} I_{core,2} \Omega_{core,2}^2 \quad (9)$$

283 because of tidal dissipation (see for instance Rieutord, 2003). As opposed  
284 to our experiments, the synchronizing system evolves from one resonance to  
285 another as the spin and orbital velocities continuously change. We suppose  
286 that the mode remains at saturation during this evolution, and thus approx-  
287 imate the tidal dissipation in the core of each body by (7) at saturation. The  
288 amplitude of the mode is given by the corresponding value of the spin-over  
289 mode determined by Lacaze et al. (2004).

290 Let's now assume that body 1 corresponds to a typical moon with a  
291 50% core orbiting a large planet (for instance Io in the vicinity of Jupiter).  
292 Then, the much heavier body 2 evolves on a much longer timescale, and  
293 the spin and core velocities of body 2 in equations (8) and (9) can be taken  
294 as constant. Besides, the angular momentum of the moon core typically  
295 corresponds to 10% of the angular momentum of its mantle, and core terms  
296 can be neglected in equations (8) and (9) to keep the problem simple. Then,  
297 using equation (8) and the third Kepler law (i.e.  $\Omega_{orbit}^2 a^3 = G(M_1 + M_2)$ ,  
298 where  $G$  is the gravitational constant) to eliminate the orbital velocity and  
299 radius, the energy equation  $dE/dt = -P_{ell}$  can easily be reduced to a single  
300 equation for the spin angular velocity

$$\frac{d\Omega_{spin,1}}{dt} = -\frac{2M_c \nu^{1/2}}{I_1} |\omega_{ell}|^{5/2} |\Omega_{spin,1} - \Omega_{orbit}|^{1/2} (\Omega_{spin,1} - \Omega_{orbit}), \quad (10)$$



$$\text{and } a = \left( a_0^{1/2} + \frac{I_1(\Omega_{spin,1}^{init} - \Omega_{spin,1})}{M_1(GM_2)^{1/2}} \right)^2, \quad \Omega_{orbit} = \left( \frac{GM_2}{a^3} \right)^{1/2}, \quad (11)$$

301 where  $M_c$  is the mass of the liquid core of body 1,  $\Omega_{spin,1}^{init}$  its initial spin-  
 302 ning angular velocity and  $a_0$  the initial orbital radius. The  $(\Omega_{spin,1} - \Omega_{orbit})$   
 303 factor on the right-hand side of equation (10) implies that the system sys-  
 304 tematically evolves towards the equilibrium state of synchronization (i.e.  
 305  $\Omega_{spin,1} = \Omega_{orbit}$ ).

306 The evolution of a typical body equivalent to Jupiter's moon Io is shown  
 307 in figure 6 for three different initial conditions. When the tidal instability is  
 308 present, the evolution takes place on very short time scales of 10000 years, and  
 309 comes from energy dissipation as large as 100 times the present dissipation by  
 310 Io's mantle. Besides, figure 6 illustrates the following general rules. A slow or  
 311 moderately fast prograde moon (i.e.  $\Omega_{spin,1}^{init}/\Omega_{orbit}^{init} > 1/3$ , solid line) always  
 312 excites elliptical instability and thus evolves rapidly towards synchronization.  
 313 A slow retrograde moon (i.e.  $\Omega_{spin,1}^{init}/\Omega_{orbit}^{init} < -1$ , dashed line) initially ex-  
 314 cites a resonance and thus evolves rapidly towards antisynchronization (i.e.  
 315  $\Omega_{spin,1} = -\Omega_{orbit}$ ), where no resonance is possible anymore. Finally, a fast  
 316 retrograde or very fast prograde moon (i.e.  $-1 < \Omega_{spin,1}^{init}/\Omega_{orbit}^{init} < 1/3$ , dotted  
 317 line) cannot excite any resonance. Note that in the last two cases, the sys-  
 318 tem should evolve because of other processes not considered here (e.g. solid  
 319 dissipation, viscous diffusion of the tidal shear, ...) and will ultimately reach  
 320 the domain of elliptical instability. However, it would be very interesting  
 321 to perform a systematic analysis of the ratio  $\Omega_{spin}/\Omega_{orbit}$  for all moons and  
 322 planets in planetary systems, in order to verify the potential impact of the  
 323 zone of slow evolution  $\Omega_{spin}/\Omega_{orbit} \in [-1; 1/3]$ .

#### 324 4. Conclusion

325 In this paper, combining theoretical and experimental approaches, we  
326 have systematically characterized the various and complex resonances excited  
327 by tidal instability in planetary liquid cores and stars, depending on their  
328 relative orbital and spinning angular velocities. We have also demonstrated  
329 that tidal instability may play a dominant role in the synchronization process  
330 of stellar and planetary binary systems. Of course, our approach is highly  
331 simplified, regarding both the structural model of the binary system as well  
332 as the estimated power dissipated by tides. Moreover, the elliptical insta-  
333 bility studied here will compete in natural configurations with various other  
334 phenomena, such as stable stratification and convection (see for instance the  
335 study of the interaction between the elliptical instability and thermal effects  
336 in Le Bars and Le Dizès, 2006), or solidification (a solid inner core ampli-  
337 fies the viscous dissipation by the generation of detached shear layers, e.g.  
338 Rieutord et al., 2001, but should appear on a longer time scale according  
339 to the orders of magnitude found here). One should also notice that our  
340 present study focus on hydrodynamical aspects of the tidal instability only,  
341 neglecting Lorentz forces related to planetary or stellar magnetic fields. This  
342 simplification is fully justified in the case of Io (see Herreman et al., 2009),  
343 but magnetic effects may be predominant in other situations. Anyway, the  
344 key point demonstrated here is that even if the tidal deformation is very  
345 small, its subsequent instability may have a velocity amplitude of first order  
346 over the whole domain and takes various and complex forms. As a result,  
347 it appears that its influence should not be neglected or oversimplified when  
348 describing the dynamics of planetary cores and stars, or when tackling other

349 problems relevant at the planetary and stellar scales, such as core cooling  
350 and dynamo process.

351

### 352 **Appendix A : notations.**

353 The operators appearing in equation (2) are defined as follows.

354 Volume terms  $\tilde{\mathcal{J}}_{i|i}$ ,  $\tilde{\mathcal{N}}_{i|j}$  and  $\tilde{\mathcal{C}}_{i|i}$  respectively correspond to the norm of  
355 mode  $i$ , to the coupling coefficient between modes  $i$  and  $j$ , and to the detuning  
356 of the instability when  $\Omega$  is slightly off the perfect resonance condition. They  
357 are computed using the scalar product

$$\tilde{\mathcal{X}}_{i|j} = \int \int \bar{\mathbf{u}}_i^0 \cdot \tilde{\mathcal{X}} \mathbf{u}_j^0 r dr dz$$

358 applied respectively to the operators

$$\mathcal{J} = \begin{pmatrix} 1 & 0 & 0 & 0 \\ 0 & 1 & 0 & 0 \\ 0 & 0 & 1 & 0 \\ 0 & 0 & 0 & 0 \end{pmatrix} \quad \mathcal{N} = \begin{pmatrix} D-1 & 0 & 0 & 0 \\ -2I & D+1 & 0 & 0 \\ 0 & 0 & D & 0 \\ 0 & 0 & 0 & 0 \end{pmatrix} \quad \mathcal{C} = \begin{pmatrix} 0 & 2\Omega & 0 & 0 \\ -2\Omega & 0 & 0 & 0 \\ 0 & 0 & 0 & 0 \\ 0 & 0 & 0 & 0 \end{pmatrix}.$$

359 Here,  $D = -\frac{\partial}{\partial r} - I \frac{\partial}{\partial \theta}$ ,  $I^2 = -1$ , and the vectors  $\mathbf{u}^0$  are defined as

$$\mathbf{u}^0 = \begin{pmatrix} u^0 \\ v^0 \\ w^0 \\ p^0 \end{pmatrix}$$

360 and correspond to the configuration without global rotation (see Lacaze et al.,  
361 2004).

362 Surface terms  $\nu_s^j$  and  $\tilde{I}_j$  respectively correspond to the viscous dissipation  
 363 close to the solid boundary estimated using the work of Kudlick (1966) and  
 364 to surface effect induced by the elliptic shape of the boundary. They are  
 365 given by

$$\begin{aligned}\tilde{I}_1 &= \int_{-1}^1 p_1^0 \left( -I \frac{(1-z^2)}{4} \frac{\partial u_2^0}{\partial r} + \frac{(1-z^2)^{1/2}}{2} v_2^0 - I \frac{z(1-z^2)}{4} \frac{\partial w_2^0}{\partial r} - I \frac{z}{4} w_2^0 \right) dz, \\ \tilde{I}_2 &= \int_{-1}^1 p_2^0 \left( I \frac{(1-z^2)}{4} \frac{\partial u_1^0}{\partial r} + \frac{(1-z^2)^{1/2}}{2} v_1^0 + I \frac{z(1-z^2)}{4} \frac{\partial w_1^0}{\partial r} + I \frac{z}{4} w_1^0 \right) dz,\end{aligned}$$

366

$$\text{and } \nu_s^j = \int_{\text{Sphere}} \nabla^* p_j^0 \cdot \mathcal{L} dS,$$

367 where  $\nabla^* = (\partial/\partial r, -Im/r, \partial/\partial z)$ ,

$$\mathcal{L} = \begin{pmatrix} -\frac{1}{2} \left( \frac{Q_+}{-p_+} + \frac{Q_-}{-p_-} \right) \\ -\frac{I}{2 \cos \phi} \left( \frac{Q_+}{-p_+} - \frac{Q_-}{-p_-} \right) \\ -\frac{\tan \phi}{2} \left( \frac{Q_+}{-p_+} + \frac{Q_-}{-p_-} \right) \end{pmatrix},$$

368

$$p_{\pm} = \frac{1 + I \operatorname{sign} \left( (1 + \Omega) \left( -\frac{\omega - m}{1 + \Omega} \pm 2 \cos \phi \right) \right)}{\sqrt{2}} \sqrt{|(1 + \Omega) \left( -\frac{\omega - m}{1 + \Omega} \pm 2 \cos \phi \right)|},$$

369

$$\text{and } Q_{\pm} = u^0 \pm I v^0 \cos \phi.$$

## 370 References

371 Aldridge, K., Seyed-Mahmoud, B., Henderson, G., van Wijngaarden, W.,  
 372 1997. Elliptical instability of the Earth's fluid core. *Phys. Earth Planet.*  
 373 *Int.* 103, 365–74.

- 374 Herreman, W., Le Bars, M., Le Gal, P., 2009. On the effects of an imposed  
375 magnetic field on the elliptical instability in rotating spheroids. *Phys. Flu-*  
376 *ids* 21, 046602.
- 377 Hollerbach, R., Kerswell, R. R., 1995. Oscillatory internal shear layers in  
378 rotating and precessing flows. *J. Fluid Mech.* 298, 327–339.
- 379 Kerswell, R. R., 1993. The instability of precessing flow. *Geophys. Astrophys.*  
380 *Fluid Dyn.* 72, 107–144.
- 381 Kerswell, R. R., 1996. Upper bounds on the energy dissipation in turbulent  
382 precession. *J. Fluid Mech.* 321, 335–370.
- 383 Kerswell, R. R., 2002. Elliptical instability. *Annual Review of Fluid Mechan-*  
384 *ics* 34, 83–113.
- 385 Kerswell, R. R., Malkus, W. V. R., 1998. Tidal instability as the source for  
386 Io’s magnetic signature. *Geophys. Res. Lett.* 25, 603–6.
- 387 Kudlick, M., 1966. On the transient motions in a contained rotating fluid.  
388 PhD thesis, MIT.
- 389 Lacaze, L., Herreman, W., Le Bars, M., Le Dizès, S., Le Gal, P., 2006. Mag-  
390 netic field induced by elliptical instability in a rotating spheroid. *Geophys.*  
391 *Astrophys. Fluid Dyn.* 100, 299–317.
- 392 Lacaze, L., Le Gal, P., Le Dizès, S., 2004. Elliptical instability in a rotating  
393 spheroid. *J. Fluid Mech.* 505, 1–22.
- 394 Le Bars, M., Le Dizès, S., 2006. Thermo-elliptical instability in a rotating  
395 cylindrical shell. *J. Fluid Mech.* 563, 189–198.

- 396 Le Bars, M., Le Dizès, S., Le Gal, P., 2007. Coriolis effects on the elliptical  
397 instability in cylindrical and spherical rotating containers. *J. Fluid Mech.*  
398 585, 323–342.
- 399 Le Dizès, S., 2000. Three-dimensional instability of a multipolar vortex in a  
400 rotating flow. *Phys. Fluids* 12, 2762–74.
- 401 Malkus, W. V. R., 1968. Precession of the Earth as the cause of geomag-  
402 netism. *Science* 160, 259–264.
- 403 Rieutord, M., 2003. Evolution of rotation in binaries: physical processes.  
404 *Stellar Rotation, Proc. IAU Symp.* 215, 394–403.
- 405 Rieutord, M., Georgeot, B., Valdettaro, L., 2001. Inertial waves in a rotating  
406 spherical shell: attractors and asymptotic spectrum. *J. Fluid Mech.* 435,  
407 103–144.
- 408 Vanyo, J. P., 1991. A geodynamo powered by luni-solar precession. *Geophys.*  
409 *Astrophys. Fluid Dyn.* 59, 209–234.
- 410 Vanyo, J. P., Likins, P. W., 1972. Rigid-body approximations to turbulent  
411 motion in a liquid-filled, precessing spherical cavity. *J. Appl. Mech.*, 39,  
412 18–24.
- 413 Waleffe, F. A., 1990. On the three-dimensional instability of strained vortices.  
414 *Phys. Fluids* 2, 76–80.

Figure 1: (a) Sketch of the experimental set-up and (b) correspondence with the geophysical configuration (top view).

Figure 2: (a) Viscous growth rate as a function of  $\Omega$ , determined analytically for the first 21 principal resonances of the  $(-1, 1)$  mode (continuous lines), of the  $(0, 2)$  mode (dashed lines) and of the  $(1, 3)$  mode (dotted lines), for fixed values of eccentricity  $\varepsilon = 0.16$  and Ekman number  $E = 1.7 \times 10^{-4}$ . Symbols stand for the location of experimentally observed resonances, with triangles corresponding to  $(-1, 1)$  modes, stars to  $(0, 2)$  modes and squares to  $(1, 3)$  modes. (b) The same for  $\varepsilon = 0.16$ ,  $E = 1.7 \times 10^{-8}$  and (c)  $\varepsilon = 0.016$ ,  $E = 1.7 \times 10^{-8}$ . Also shown in (c) is the approximated growth rate given by equation (3), using two extreme values  $c = 0$  and  $c = 10$ . Note that in the limit  $\sqrt{E}/\varepsilon \ll 1$ , resonance bands are dense in the  $\Omega$  space, except in the stable range  $\Omega \in [-3/2; -1/2]$ . The false impression that holes without resonance could be created in (c) only comes from the fact that we restrain our computations to the first 63 resonances.

Figure 3: Time sequence of the periodic  $(0, 2)$  mode excited in our experiment for  $\varepsilon = 0.16$ ,  $E = 4.5 \times 10^{-4}$  and  $\Omega = -0.20$  (i.e.  $\Omega_F = 4.7\text{rad/s}$  and  $\Omega_{orbit} = -0.94\text{rad/s}$ ).

Figure 4: Spatiotemporal diagrams obtained by extracting the same line parallel to the rotation axis in each image of a given video sequence: (a)  $(0, 2)$  mode excited in our experiment for  $\varepsilon = 0.16$ ,  $E = 4.5 \times 10^{-4}$  and  $\Omega = -0.20$  (i.e.  $\Omega_F = 4.7\text{rad/s}$  and  $\Omega_{orbit} = -0.94\text{rad/s}$ ) and (b)  $(1, 3)$  mode excited in our experiment for  $\varepsilon = 0.16$ ,  $E = 3.4 \times 10^{-4}$  and  $\Omega = -0.11$  (i.e.  $\Omega_F = 6.2\text{rad/s}$  and  $\Omega_{orbit} = -0.68\text{rad/s}$ ). The measured mode pulsations are respectively  $\omega = 4.4\text{rad/s}$  and  $\omega = 12.6\text{rad/s}$ , in good agreement with the theoretical predictions.

Figure 5: *Kalliroscope visualization of the elliptical instability for a fixed Ekman number  $E = 10^{-5}$  and increasing values of  $\varepsilon$  (note that these four pictures were obtained in a 20cm in diameter sphere). The effective rotation axis of the fluid is clearly visible, coming from the superimposition of the imposed vertical rotation and the spin-over mode. Hence, the inclination angle is an indication of the ratio between the mode amplitude and the imposed rotation. It seems to saturate for  $\varepsilon/\sqrt{E} > 0(10)$ , where the instability induces velocity perturbations comparable to the imposed rotation velocity. Further increasing  $\varepsilon$ , the flow becomes more and more complex at small scale where disordered motions take place. However, the spin-over mode remains present at large scale. The same behavior is observed when decreasing the Ekman number. Such an organization of the flow with a large scale excited mode with first order velocities and superimposed three dimensional turbulence is expected at the planetary scale, for instance in Io's core.*

Figure 6: *Evolution of a typical moon corresponding to Io under the influence of Jupiter's tides (i.e.  $M_1 = 8.93 \times 10^{22} \text{kg}$ ,  $M_2 = 1.90 \times 10^{27} \text{kg}$ ,  $a_0 = 421800 \text{km}$ ,  $R_1 = 1840 \text{km}$  with a 50% core,  $I_1 = 1.2 \times 10^{35} \text{kg.m}^2$ ,  $\nu = 10^{-6} \text{m}^2 \text{s}^{-1}$ ) for three different initial spinning angular velocities, corresponding to a slow prograde moon ( $\Omega_{\text{spin},1}^{\text{init}}/\Omega_{\text{orbit}}^{\text{init}} = 4$ , solid line), to a slow retrograde moon ( $\Omega_{\text{spin},1}^{\text{init}}/\Omega_{\text{orbit}}^{\text{init}} = -4$ , dashed line) and to a rapid moon ( $\Omega_{\text{spin},1}^{\text{init}}/\Omega_{\text{orbit}}^{\text{init}} = 1/4$ , dotted line): (a) evolution of the distance between Io and Jupiter in comparison with the initial distance  $a_0 = 421800 \text{km}$ , (b) evolution of the ratio between the spin and orbital angular velocities and (c) dissipated power by the elliptical instability.*



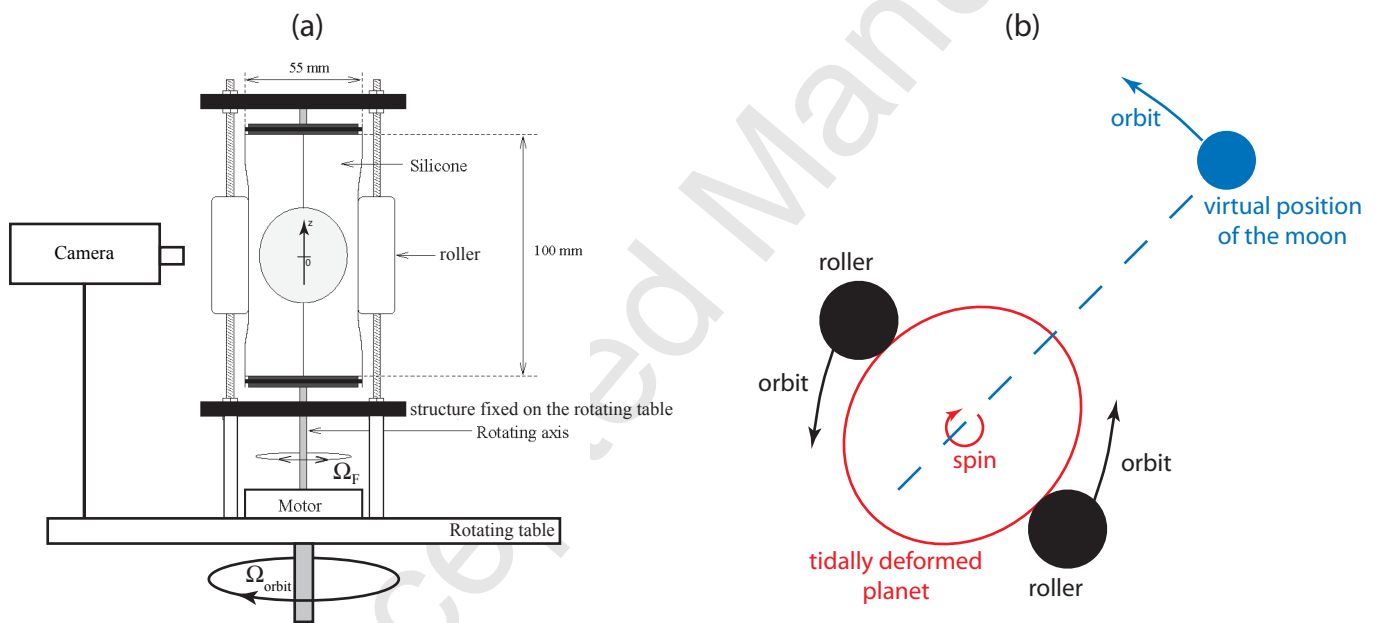


Figure 1

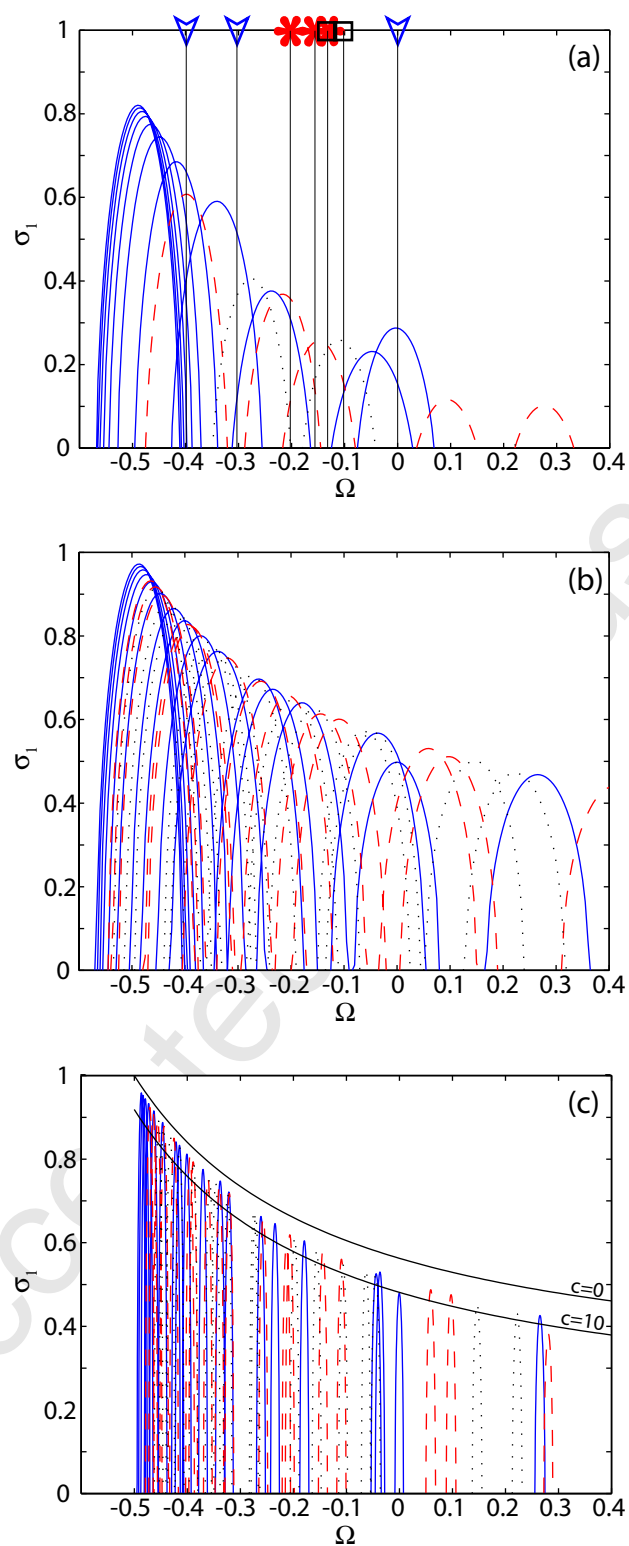


Figure 2

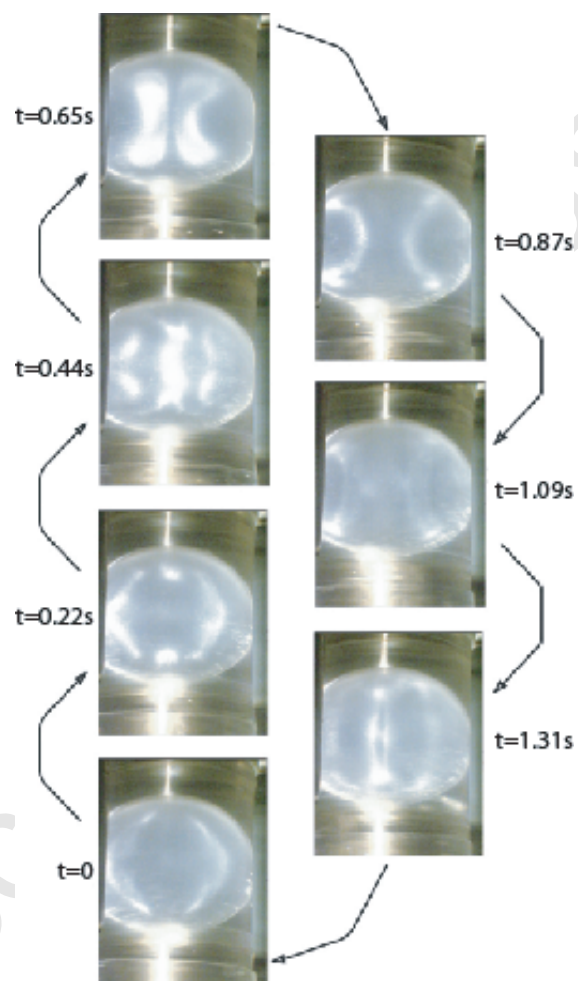


Figure 3

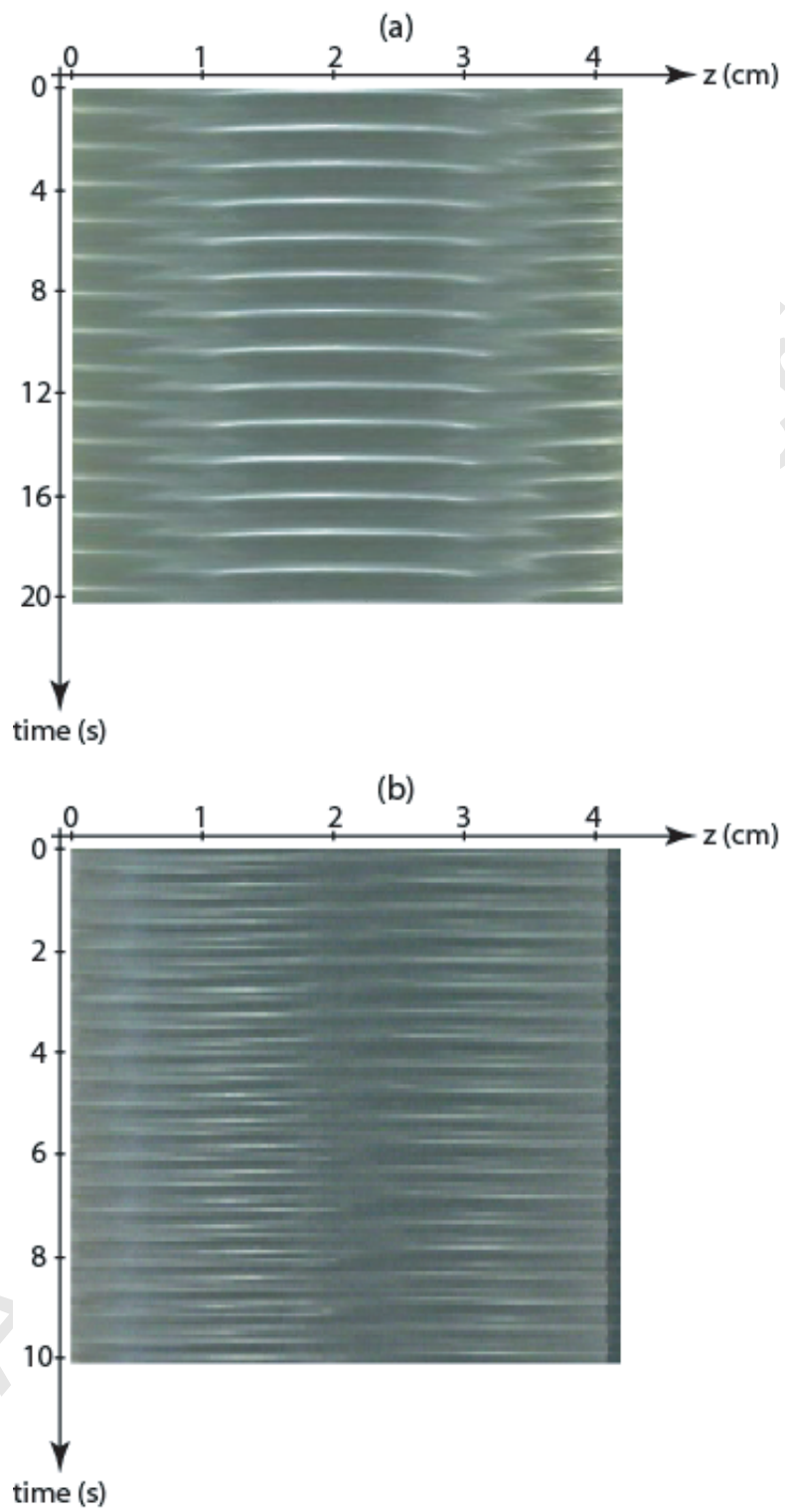


Figure 4

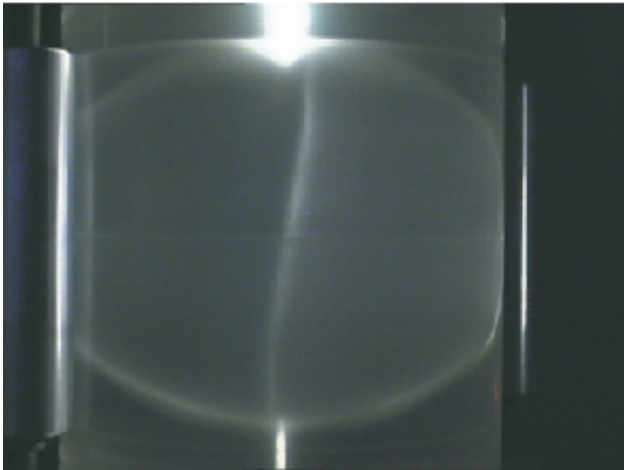
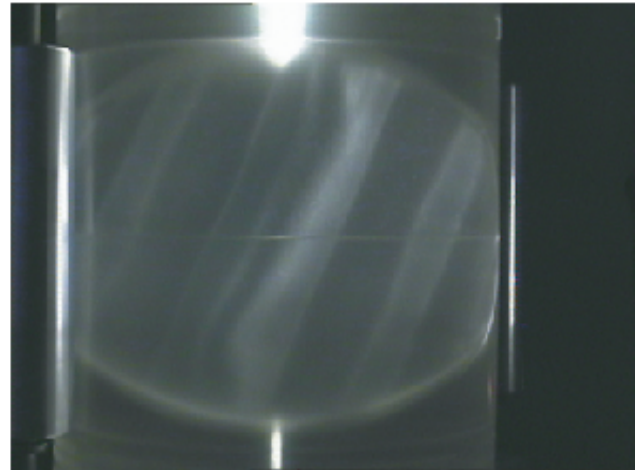
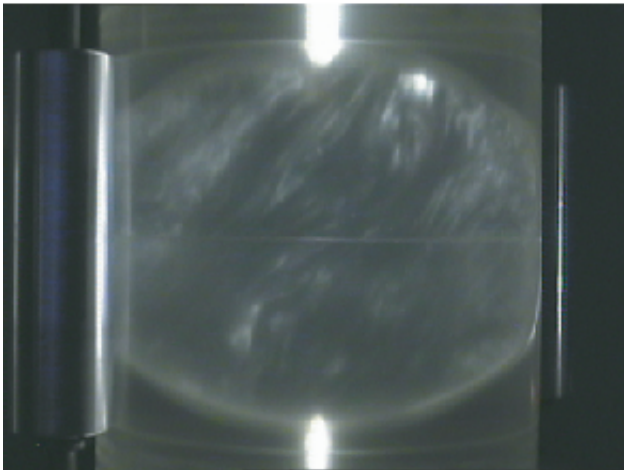
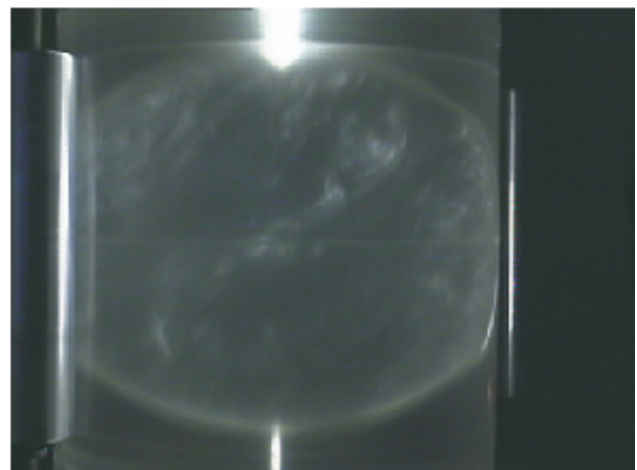
(a)  $\epsilon=0.03$ (b)  $\epsilon=0.04$ (c)  $\epsilon=0.05$ (d)  $\epsilon=0.06$ 

Figure 5

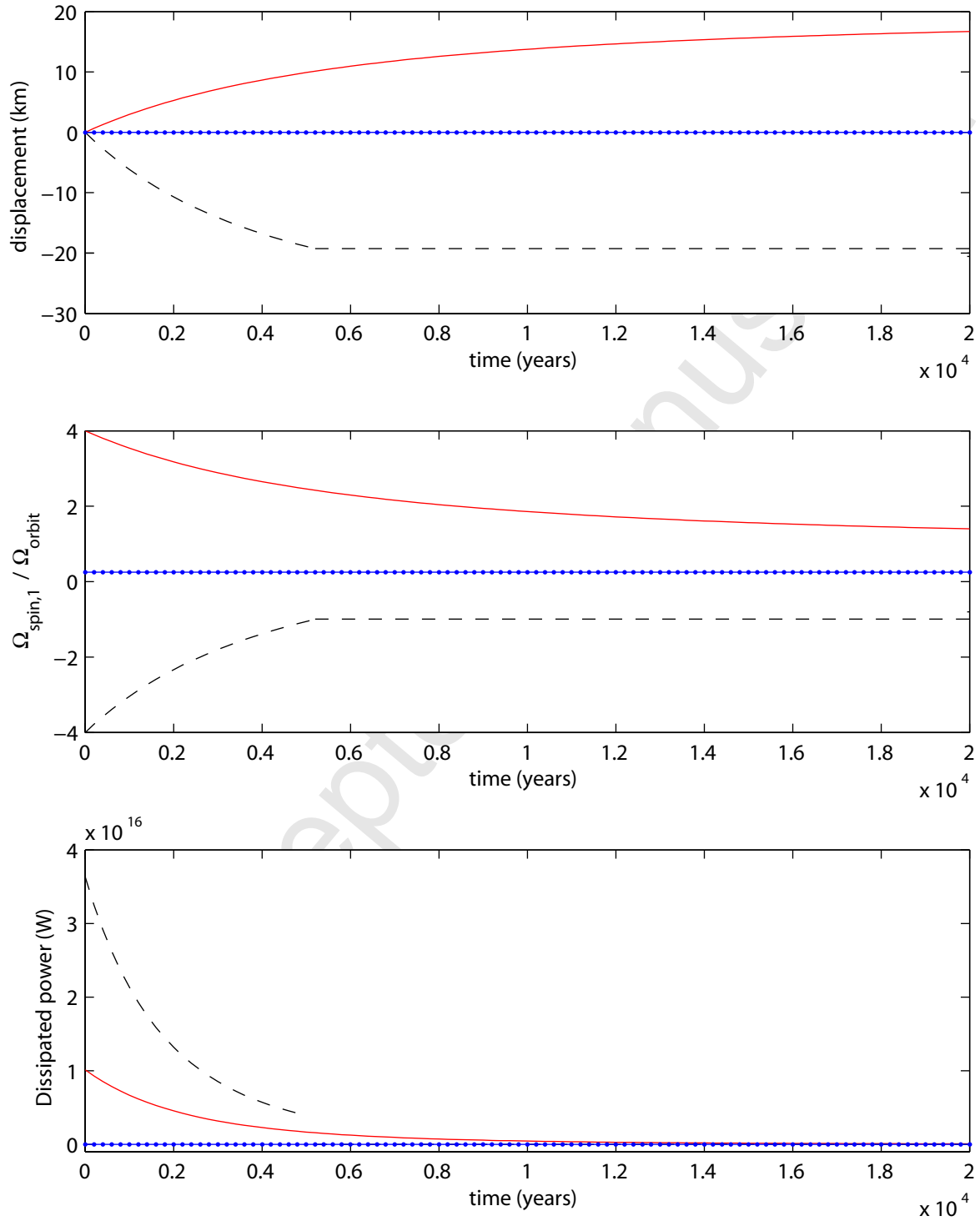


Figure 6